

Metasomatic origin of garnet orthopyroxenites in the subcontinental lithospheric mantle underlying Pali Aike volcanic field, southern South America

Jian Wang · Keiko H. Hattori · Charles R. Stern

Received: 19 December 2007 / Accepted: 16 July 2008 / Published online: 1 August 2008
© Springer-Verlag 2008

Abstract Garnet-bearing orthopyroxenites occur as both discrete xenoliths and as veinlets in peridotite xenoliths that were brought to the surface by Quaternary Pali Aike alkali basalts in the southernmost of the Patagonian plateau lava fields in southern South America. Orthopyroxenites commonly contain Ti-rich minerals and also relict grains of olivine (Ol) and clinopyroxene (Cpx) occurring as inclusions in secondary orthopyroxene (Opx). The secondary Opx contains high TiO₂ (0.20–0.59 wt.%), moderate Al₂O₃ (2.87–5.10 wt.%) and low magnesium numbers (Mg#, 84.5–89.2) compared with Opx in garnet-bearing peridotites. This suggests that secondary Opx formed at the expense of Ol and Cpx during metasomatism by an evolved Ti-rich melt. The orthopyroxenites contain bulk-rock concentrations of Cr, Ni and platinum group elements similar to peridotites, suggesting that these metals were essentially immobile during metasomatism, and that the metasomatizing melt did not introduce these elements. Instead, the metasomatizing melt contributed alkalis, Ti, Si, Al, and S to the orthopyroxenites based on increased concentrations of

these elements and mineralogy. Secondary Opx has also been documented in mantle peridotite xenoliths derived from beneath both active arcs and ancient cratons. In comparison with such Opx in these mantle samples, the secondary Opx in the Pali Aike xenoliths contains relatively high Ti and Al and low Mg. High Ti and low Mg in these samples reflect the evolved nature of the metasomatizing melt that originated from the underlying asthenospheric mantle. The type of secondary Opx, typified by these samples, may be common elsewhere in subcontinental mantle lithosphere (SCLM) affected by asthenospheric upwelling.

Introduction

The occurrence of secondary orthopyroxene (Opx) has been documented in peridotite xenoliths derived from subarc mantle wedges and has been interpreted as resulting from Si enrichment by aqueous fluids and melts derived from subducting slabs (e.g., Kelemen 1986, 1990; Smith et al. 1999; Arai and Kida 2000; Prouteau et al. 2001; Kilian and Stern 2002; Arai et al. 2003, 2004). The high modal abundance of Opx, and the high Ni and Mg# of garnet (Grt) orthopyroxenite in SCLM underlying Archean cratons (e.g., Kaapvaal, North China) are also explained by infiltration of Si-rich melt (Kesson and Ringwood 1989; Kelemen et al. 1998; Zhang et al. 2001; Bell et al. 2005; Chen and Zhou 2005; Liu et al. 2005; Malaspina et al. 2006). This Si-rich melt is commonly considered to be derived from an old subducting slab or delaminated lower crust (Arth and Hanson 1975; Rapp et al. 1991; Gao et al. 2004; Chen and Zhou 2005).

An alkali-rich melt, in contrast, has a low activity of SiO₂ and is not expected to cause Si enrichment in mantle peridotites. Nevertheless, a recent study of xenoliths in

Editorial handling: R. Abart

J. Wang (✉)
College of Earth Sciences, Jilin University,
Changchun, Jilin, 130061, People's Republic of China
e-mail: jian.wang1205@gmail.com

J. Wang · K. H. Hattori
Department of Earth Sciences, University of Ottawa,
Ottawa, Ontario, Canada, K1N 6N5

K. H. Hattori
e-mail: khattori@uottawa.ca

C. R. Stern
Department of Geological Sciences, University of Colorado,
Boulder, CO, 80309-0399, USA
e-mail: Charles.Stern@colorado.edu

western Japan by Arai et al. (2006) suggests that evolved alkali-rich melt is in fact capable of producing Si enrichment in such peridotites. Ertan and Leeman (1996) also documented the formation of phlogopite-bearing orthopyroxenite in harzburgites during the metasomatism by high-K melt in the Cascades subarc mantle.

This paper reports the bulk rock compositions, including platinum group elements, and the mineralogy and mineral chemistry of Grt-bearing orthopyroxenites from Quaternary alkali basalts in the Pali Aike area, southern South America (Fig. 1). These data, combined with the textures of rocks and minerals, indicate that orthopyroxenites formed from Grt peridotites during the injection of asthenospheric mantle-derived, Ti-rich melt genetically associated with the Pali Aike alkali basalts.

Geological background and petrological description of the xenoliths from Pali Aike

The modern geological framework of South America results mainly from the subduction of the Nazca and Antarctic plates beneath the South American continent (Fig. 1; D'Orazio et al. 2000). The Chile ridge between the Nazca and Antarctic plates collided with the trench near the southern tip of South America at ~14–15 Ma (Cande and Leslie 1986), and the eastern extension of this ridge was then

subducted beneath the South American continent. Ridge subduction was responsible for the formation of a slab window, which produced the extensive Patagonian plateau basalts in the interior of southern South America (Ramos and Kay 1992; Gorrington et al. 1997; Gorrington and Kays 2001). The plateau basalts, which are considered to have originated from the underlying asthenospheric mantle through a slab window (e.g., Gorrington et al. 1997), are younger to the northeast, with ages ranging from ~12 Ma to recent, following the track of the subducted ridge. The Pali Aike volcanic field is the southernmost plateau basalt field, covering 45×100 km² (Fig. 1), but it is young in age (≤4 Ma). The time delay for its origin after ridge subduction has been explained with the hypothesis that an extensional tectonic regime, favorable to the ascent of the magmas, was present in Pali Aike area only after 6 Ma (D'Orazio et al. 2000).

The Pali Aike volcanic field contains alkali basaltic lavas as well as pyroclastic rocks, which include tuff breccias associated with maars and both spatter and scoria cones. Pyroclastic rocks contain peridotite and pyroxenite xenoliths (Skewes and Stern 1979; Kempton et al. 1999a, b; Stern et al. 1999; D'Orazio et al. 2000), the latter of which are the focus of this study. The pyroxenite samples analyzed in this study were collected from both a small scoria cone (samples BN and BNC; 52°02'23" S and 70°04'08" W), and from the tuff ring around the maar (samples BNH) within which this cone occurs. These sample sites are located at the southeast end of a chain of maars and cones aligned along a NW–SE fissure, just north of the north branch (Brazo Norte) of the Seco (dry) river. Peridotite samples were collected from both these same sites and from other maars, such as the one that encloses Timone lake (samples TM; 52°00'58" S and 70°12'16" W) to the northwest.

General petrography of samples

Pali Aike xenolith samples are divided into two types based on their mineralogy and textures; peridotites and pyroxenites. The peridotites are garnet- and spinel-bearing lherzolites and harzburgites and further divided into four subtypes based on the presence or absence of Grt: Grt–Spl lherzolite, Spl lherzolite, Grt–Spl harzburgite, and Spl harzburgite (Stern and Skewes 1979; Kempton et al. 1999a, b; Stern et al. 1999). Modal and cryptic metasomatism is common especially in Grt-bearing samples. Modal metasomatism produced Ti-rich phlogopite, Ti-rich amphibole (Ti–Amp), Mg-rich ilmenite (Mg–Ilm), orthopyroxene and minor sulphides. Discontinuous veinlets (<3 mm) composed of Ti–phlogopite and/or Mg–Ilm, with orthopyroxene-rich halos, are common in Grt-bearing harzburgites.

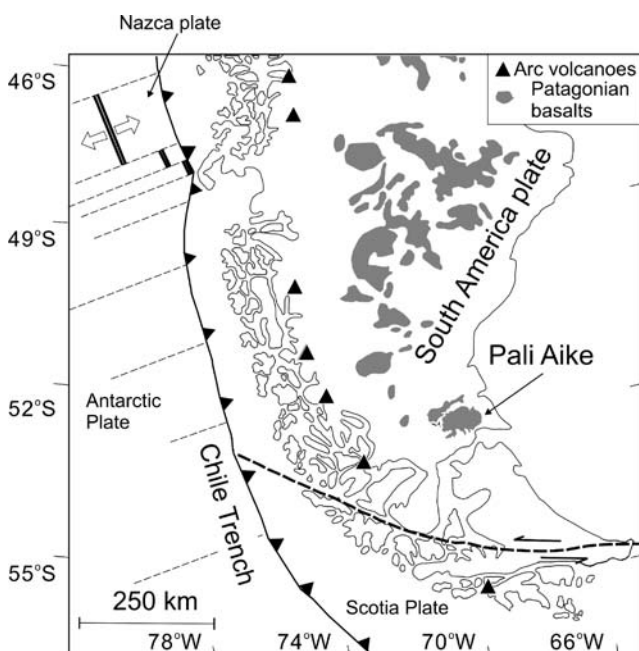


Fig. 1 Map of southern South America, showing the locations of the Quaternary alkali basalt fields of Pali Aike and other late Cenozoic basalts of Patagonian plateau. Also shown are volcanoes of the Andean Austral Zone (AVZ; modified after Stern et al. 1999)

Table 1 Representative compositions of minerals in garnet orthopyroxenites from Pali Aike

Sample phase host	BN46						BNH5						BN43		
	Opx-C	Opx-R	Opx-f	Grt	Cpx Opx	Ti-Phl	Opx-C	Opx-R	Opx-f	Cpx-C Opx	Cpx-R	Grt	Spl Grt	Ol-C Opx	Ol-R Opx
SiO ₂	56.25	56.62	56.21	41.94	52.45	38.68	55.89	56.08	55.58	52.62	53.26	41.99	0.02	40.03	39.99
TiO ₂	0.37	0.32	0.36	0.20	1.07	5.23	0.26	0.40	0.38	0.65	1.04	0.18	0.48	0.06	<0.04
Al ₂ O ₃	3.17	3.12	3.00	23.27	5.73	16.21	3.64	3.62	3.61	5.51	5.77	23.89	57.82	0.03	0.04
Cr ₂ O ₃	0.15	0.13	0.09	0.46	0.31	0.33	0.35	0.30	0.28	0.39	0.44	0.39	7.29	<0.03	0.05
FeO (t)	9.51	9.04	9.84	11.84	5.12	6.19	7.69	7.83	8.02	3.96	4.02	9.61	14.18	12.20	12.33
MnO	0.13	0.13	0.18	0.38	0.11	<0.03	0.06	0.08	0.11	0.06	0.06	0.30	<0.03	0.13	0.10
MgO	30.73	30.81	30.55	18.58	14.67	18.99	31.75	31.76	32.39	15.12	14.84	20.11	19.69	47.05	46.85
CaO	0.81	0.82	0.83	4.82	18.51	0.07	0.56	0.58	0.54	17.32	17.57	4.03	<0.01	0.06	0.10
Na ₂ O	0.13	0.11	0.15	0.03	2.19	0.75	0.12	0.12	0.19	1.86	1.83	0.05	0.02	0.02	0.03
NiO	0.08	0.11	0.03	0.02	0.03	<0.01	0.16	0.14	0.27	<0.03	0.05	0.03	0.44	0.33	0.40
K ₂ O						9.17									
Cl						0.02									
F						0.18									
Total	101.3	101.2	101.2	101.5	100.2	95.81	100.5	100.9	101.4	97.48	98.87	100.6	99.94	99.91	99.90
Mg# ^b	85.2	85.9	84.7	73.7	83.6	84.6	88.0	87.9	87.8	87.2	86.8	78.9	76.0	87.3	87.1
Cr# ^c													7.8		

Total Fe as FeO

Ol olivine, Opx orthopyroxene, Cpx clinopyroxene, Ilm ilmenite, Grt garnet, Phl phlogopite, Amp amphibole, Spl spinel, C core of coarse grain, R rim of coarse grain, f fine grain along grain boundaries or forming aggregates

^aVeinlet of garnet-bearing orthopyroxenite in BN92

^bMg# = $100 \times \text{Mg} / (\text{Mg} + \text{total Fe})$ for all minerals except for spinel. Mg# for spinel is $100 \times \text{Mg} / (\text{Mg} + \text{Fe}^{2+})$ in which Fe²⁺ is calculated assuming stoichiometric composition

^cCr# = $100 \times \text{Cr} / (\text{Cr} + \text{Al})$

Pyroxenite xenoliths are mainly orthopyroxenites with minor websterites. Garnet is lacking in most websterite samples, suggesting their formation at relatively shallow levels. All orthopyroxenite samples, described in more detail below, contain Grt, as well as in many cases Ti-rich phlogopite, Ti-rich amphibole (Ti–Amp), Mg-rich ilmenite (Mg–Ilm) and minor sulphides, and are mineralogically similar to the modal metasomatic veins found in garnet peridotites.

Analytical method

Mineral compositions were determined by a Camebax MBX microprobe at Carleton University using 15 kV accelerating voltage, 20 nA beam current, focused beam size (<1 μm), and natural and synthetic mineral standards. A counting time of 20s was used for all elements except 50s for Ca in Ol and 60s for F in phlogopite. Compositions for a specific mineral in individual samples show a narrow range. Therefore only representative analyses of minerals are listed in Table 1.

For bulk rock analysis, the rims of xenoliths that have been affected by either the host basalt and/or

weathering were removed. Major and minor elements were determined using a Philips PW 2400 X-ray fluorescence spectrometer after fusing the sample powder with LiBO₃ at the University of Ottawa. Precision based on replicate runs of eleven samples is ±0.35% for Al₂O₃, ±0.48% for MgO, ±1.3% for Cr, ±9.2% for Ni. The accuracy, which was monitored using references of MRG-1 and Sy-2, shows ±0.039% for Al₂O₃, 0.28% for MgO, 3.4% for Cr, 4.0% for Ni. Precision and accuracy are less than 1% and 10% for other major and minor elements, respectively.

Platinum group elements (PGE) were determined by isotopic dilution using a mixed spike of ¹⁹⁰Os, ¹⁹¹Ir, ⁹⁹Ru, ¹⁹⁴Pt and ¹⁰⁵Pd. Platinum group elements with a spike were pre-concentrated into a Ni bead and dissolved in concentrated HNO₃. The analytical procedures are similar to those by Ravizza and Pyle (1997). Mass ratios were determined using an Agilent HP-4500 ICP-MS at the University of Ottawa. Blank contributions were 0.002–0.006 ng Os/g flux, 0.002–0.007 ng Ir/g flux, 0.02 ng Ru/g flux, 0.07–0.16 ng Pt/g flux and 0.03–0.12 ng Pd/g flux. The blanks are negligible compared to the amounts in samples; thus, blank corrections were not applied to the results. Precisions of PGE determination are <15% for Os, <14% for Ir, <12%

Table 1 (continued)

Sample phase host	BN43			BN05					BNC1							BNC2	
	Ol-f	Opx-C	Opx-R	Ol-C	Ol-R	Opx-C	Opx-R	Grt	Opx			Ol-f	Opx-C	Opx-R	Opx-f	Cpx-f	Ol-f
									Ol-C	Ol-R	Grt						
SiO ₂	39.96	54.25	55.33	40.91	41.05	55.52	55.40	42.45	40.81	40.97	40.97	55.19	54.84	55.38	51.60	39.92	
TiO ₂	<0.04	0.31	0.36	<0.04	0.07	0.30	0.42	0.42	0.07	0.06	0.08	0.44	0.43	0.46	1.42	0.12	
Al ₂ O ₃	0.06	3.64	3.75	0.04	0.04	3.77	4.10	23.36	0.06	0.04	0.07	4.01	4.01	4.00	6.60	0.06	
Cr ₂ O ₃	<0.03	0.28	0.31	<0.03	0.03	0.48	0.38	0.97	<0.03	<0.03	0.03	0.33	0.35	0.33	1.01	<0.03	
FeO (t)	12.99	7.77	7.83	13.24	13.44	8.29	8.69	9.19	13.11	13.55	13.61	8.45	8.56	8.43	4.58	15.42	
MnO	0.14	0.14	0.13	0.09	0.13	0.12	0.11	0.32	0.14	0.15	0.05	0.24	0.23	0.20	0.06	0.19	
MgO	47.36	32.11	32.33	46.27	46.35	31.41	31.34	20.32	46.76	46.48	46.08	31.79	31.34	31.66	14.83	44.11	
CaO	0.08	0.58	0.61	0.11	0.17	0.78	0.78	3.99	0.09	0.10	0.10	0.72	0.82	0.81	17.37	0.09	
Na ₂ O	0.04	0.17	0.16	<0.02	0.03	0.12	0.16	0.10	0.04	<0.02	0.03	0.20	0.20	0.22	2.18	<0.02	
NiO	0.34	0.22	0.22	0.41	0.48	0.15	0.09	0.00	0.47	0.37	0.33	0.06	0.14	0.17	0.17	0.36	
K ₂ O																	
Cl																	
F																	
Total	101.0	99.46	101.0	101.1	101.8	100.9	101.5	101.1	101.6	101.7	101.4	101.4	100.9	101.7	99.83	100.3	
Mg# ^b	86.7	88.1	88.0	86.2	86.0	87.1	86.5	79.8	86.4	85.9	85.8	87.0	86.7	87.0	85.2	83.6	
Cr# ^c																	

for Ru, <11% for Pt and <19% for Pd based on repeat analyses of five samples. Accuracy of PGE determination is less than 10% based on repeated analyses of a reference (JP-1).

The contents of S were determined using a Varian Vista-Pro inductively coupled plasma atomic emission spectrometer after digestion of ~0.2 g powder sample with aqua regia in a screw-top Teflon vial at ~130°C for 48 h. The precision of S based on replicate runs of five samples is <5%. The detection limit for S is 4.5 ppm.

Garnet orthopyroxenite

Petrography

Garnet orthopyroxenites are dark brown in hand specimens and are distinctly different in appearance from light green colored peridotites. They occur either as discrete xenoliths or in veinlets (>5 mm) in harzburgites (BN92; Fig. 2a) and/or lherzolites. Discrete orthopyroxenite xenoliths contain small angular peridotite fragments (5 to 10 mm in size) and these fragments show diffuse boundaries with the orthopyroxenite host. Orthopyroxenites show equigranular and/or porphyroblastic texture with coarse Grt (up to 5 mm) and Opx (up to 4 mm). They are composed of Opx (≥85 vol.%), Grt (1–5 vol.%), Ol (≤1 vol.%), Cpx (≤1 vol.%), Ti-phlogopite, Ti-Amp, Mg-Ilm, and minor sulphide minerals (Ni-bearing pyrrhotite, pentlandite, cubanite, and chalcopyrite).

Olivine, Cpx, and spinel in orthopyroxenites are interpreted as the primary peridotite minerals as they are

commonly enclosed by poikilitic Opx and Grt. Olivine occurs as inclusions within coarse Opx (Fig. 2d) and as interstitial grains along boundaries of minerals (Fig. 2b,c). Clinopyroxene is minor (<5 vol.%) and found only in four samples (BNH5, BNH13, BNC1, BN46). Optically continuous relict Cpx grains occur as inclusions in secondary Opx (Fig. 2e) and Grt. It also forms narrow (<200 μm) bands along secondary Opx (Fig. 2f).

Secondary Opx is fine (<0.3 mm) to coarse (>2 mm) and characterized by variable shape, no cleavages, and cloudy appearance due to abundant fluid inclusions (Fig. 2d). Fine-grained Opx forms aggregates in coarse-grained Opx, and bands along boundaries of other minerals. In some cases, secondary Opx shows granular re-crystallization texture with ~120° triple junctions (Fig. 2e). Clear Opx without fluid inclusions are considered as primary. They are tabular in form and coarse-grained (>2 mm), and display well developed cleavages. The compositions of primary and secondary Opx are similar in individual samples, suggesting that Opx grains have chemically re-equilibrated.

Garnet usually occurs as isolated large grains (up to 5 mm) and commonly contains inclusions of rounded spinel and corroded Cpx. Several samples (BNC1, BNC2, BNC3, BN43) contain Grt grains which have decomposed into kelyphite assemblages consisting of extremely fine-grained spinels, pyroxenes and hydrous phases. These kelyphites may have formed as a result of decompression during transport of xenoliths to the surface. Ti-phlogopite and Mg-Ilm are minor to rare, but occur in all Grt orthopyroxenites. They commonly form discontinuous and irregular narrow (<2 mm) veinlets. Coarse-grained phlogopite commonly encloses rounded secondary Opx. Ti-Amp is rare and locally occurs as thin

BNC2					BN92 ^a				BNH13						
Opx	Spl-C	Spl-R	Ti-Amp	Ti-Phl	Ol-f	Opx-f	Cpx-f	Mg-Ilm	Opx						
									Ol-C	Ol-R	Ol-f	Cpx-f	Opx-C	Opx-R	Ti-Amp
54.34	0.15	0.17	54.07	37.38	41.12	54.93	52.03	0.00	40.53	41.41	40.66	51.13	56.41	55.50	56.04
0.43	0.73	0.74	4.83	7.13	<0.04	0.45	1.59	55.09	<0.04	<0.04	<0.04	1.42	0.23	0.20	3.38
3.80	59.42	61.57	15.38	15.18	0.02	4.18	6.33	1.38	0.00	0.02	0.02	7.55	3.27	3.61	19.24
0.30	4.43	3.30	0.03	0.60	<0.03	0.42	0.34	1.84	<0.03	<0.03	<0.03	0.72	0.31	0.36	0.01
9.71	15.42	13.92	5.24	6.69	11.13	7.12	3.96	26.89	12.95	12.96	12.19	4.04	8.06	8.16	5.04
0.17	0.17	0.09	0.06	0.04	0.13	0.12	0.07	0.34	0.13	0.10	0.09	0.06	0.10	0.13	0.12
30.17	19.59	20.64	3.58	17.37	47.20	31.74	14.58	13.66	45.94	46.54	46.12	14.18	31.10	31.24	3.23
0.76	0.01	0.02	5.87	0.04	0.08	0.73	19.44	0.02	0.05	0.05	0.08	18.79	0.66	0.64	7.31
0.23	0.01	0.02	3.28	0.59	<0.02	0.11	1.73	0.01	<0.02	0.02	0.02	1.84	0.15	0.16	0.98
0.09	0.35	0.30	0.15	0.20	0.34	0.11	0.17	0.24	0.44	0.41	0.41	0.05	0.13	0.11	0.01
			5.65	9.85											1.53
			0.00	0.02											0.10
			0.04	0.28											0.16
99.99	100.3	100.8	98.18	95.49	100.0	99.91	100.2	99.46	100.0	101.5	99.63	99.77	100.4	100.1	97.13
84.7	74.5	77.1	55.0	82.2	88.3	88.8	86.8	47.5	86.3	86.5	87.1	86.2	87.3	87.2	53.3
	4.8	3.5													

veinlets surrounding Ol, Cpx or spinel, and it is commonly associated with fine-grained Mg–Ilm.

Spinel occurs either as inclusions in Grt with narrow reaction rims (less than 5 μm) or as individual grains surrounded by Ti–Amp and Opx (Fig. 2g). Sulphides are minor, but present in all orthopyroxenite samples. Sulphides form spherical to globular grains (up to 200 μm) and are commonly associated with phlogopite or Amp and enclosed by Opx and Ol (Fig. 2h). The globular shape of sulphides suggests that sulphides were once liquid and that immiscible sulphide liquid was likely present in the metasomatizing agent. Most sulphide grains are homogeneous Ni-bearing pyrrhotite (Fe_{1-x}S , <20 wt.% Ni). Several pyrrhotite grains contain exsolved phase of pentlandite ($(\text{Ni}, \text{Fe}, \text{Co})_9\text{S}_8$) or cubanite (CuFe_2S_3). These exsolved phases form flames, lamellae and bands close to the margins of sulphide grains (Fig. 2h). Sulphide grains commonly contain minor (<5 vol. %) oxide with Fe and minor Cu in their margins (Fig. 2h). A similar occurrence of oxides has been reported within globular sulphide grains in volcanic rocks and mantle peridotites, and has been interpreted as an exsolution product of sulphide liquid (e.g., Francis 1990; Hattori et al. 2002), since O may replace up to 50% of S in sulphide liquid (Gaetani and Grove 1997; Rose and Brenan 2001).

Orthopyroxenite veinlets contain the same mineral assemblage as orthopyroxenite xenoliths, but grain size is smaller (<0.5 mm) in veinlets. The veinlets have diffuse boundaries with the host peridotites and are accompanied by halos of secondary Opx (Fig. 2a). These secondary Opx grains are distinctly different from primary Opx because the secondary Opx is cloudy due to abundant fluid inclusions (Fig. 2d).

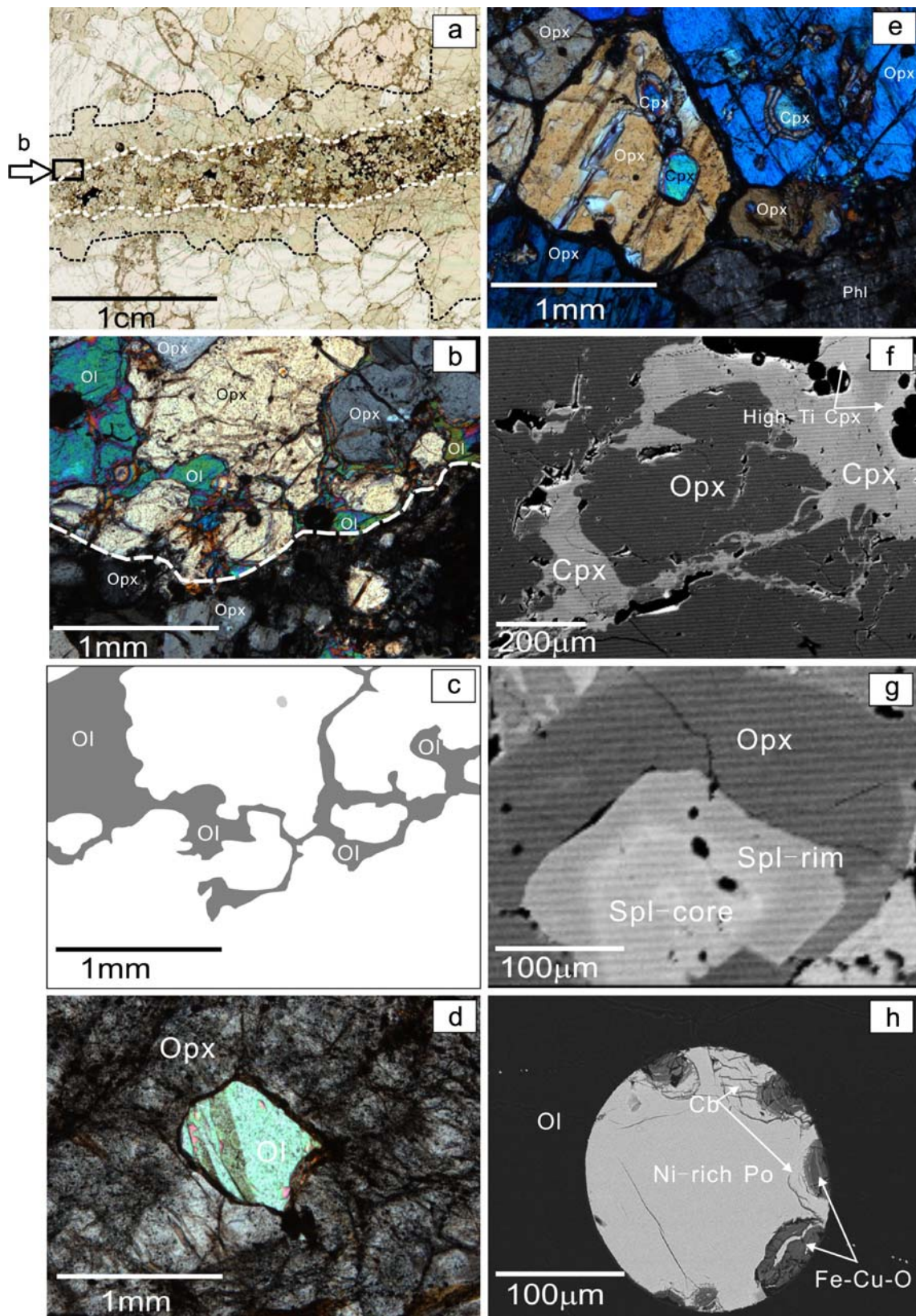
Relict grains of Ol are common in veinlets and some are optically continuous with Ol grains outside the veinlets (Fig. 2b,c).

Mineral chemistry of orthopyroxenites

Olivine compositions are similar within and between grains in individual samples (Table 1), suggesting that Ol has generally attained equilibration excluding one case described below. Olivine in orthopyroxenites has lower Mg (Fo=83.3–87.3) and about the same range of NiO contents (0.33–0.53 wt.%) compared with Ol in peridotites; Fo 87.1–89.3 and 0.38–0.48 wt.% NiO for Ol in Grt–Spl harzburgite, and Fo 89.1–90.6 and 0.32–0.41 wt.% NiO for Ol in Grt–Spl lherzolite (Table 1, Fig. 3). One Ol inclusion in Opx in sample BNH13 contains high Fo, 90.1, which is higher than other grains (Fo, ~87) in the same sample, implying this grain keeps the original composition and was not in equilibrium with other relict Ol and secondary Opx.

Clinopyroxene is considered as a relict mineral, but it is variably enriched in TiO_2 (0.65–1.59 wt.%), lowered in Mg# ($100 \times \text{Mg}/[\text{Mg} + \text{total Fe}] = 82.6–90.7$) and Cr_2O_3 (0.25–1.16 wt.%) compared to Cpx in peridotites. Furthermore, single grains of Cpx shows compositional variations in Ti and MgO contents, suggesting that the Cpx compositions are modified during the metasomatism and not equilibrated.

Spinel grains show small compositional variations of Cr and Al within individual grains. X_{Mg} ($=\text{Mg}/[\text{Mg} + \text{Fe}^{2+}]$) of spinel inclusions in Grt in sample BNH5 range from 0.705 to 0.761, and individual grains of BNC2 from 0.745 to



◀ **Fig. 2 a** Photograph of an orthopyroxenite veinlet in Grt–Spl harzburgite (sample BN92). The veinlet (shown with *white dashed lines*) is accompanied by metasomatic halos (outer margins shown with *black dashed lines*). Red garnet, opaque minerals ilmenite, yellow green orthopyroxene, and transparent olivine. Square in the middle left, at the contact between veinlet and halo, is shown in **b**. **b** Photomicrograph of the square in **a** between crossed polarizers. Optically continuous relict olivine (Ol) grains occur in and along Opx grains and across the boundary of veinlet. The boundary of the veinlet and the metasomatic halo is shown with a *thick white dashed line*. Note the texture suggests that the veinlets were the foci of the injection of a metasomatic agent that resulted in the replacement of Ol by Opx. **c** The outlines of the relict Ol grains shown in **b**. **d** Photomicrograph of orthopyroxene (Opx) enclosing a relict Ol grain in orthopyroxenite (sample BNC1). Note cloudy secondary Opx with abundant fluid inclusions. **e** Photomicrograph of secondary Opx enclosing relict clinopyroxene (Cpx) in orthopyroxenite between crossed polarizers (sample BN46). Note the $\times 120^\circ$ angle at triple junctions of grain boundaries of the secondary Opx in the upper part of the photograph. **f** Back-scattered electron image of a narrow ($<200 \mu\text{m}$) band of relict Cpx along newly formed Opx. Note the bright parts in the Cpx are high in Ti and low in Mg compared to darker parts. **g** Back-scattered electron image of a zoned spinel enclosed in secondary Opx in orthopyroxenite (sample BNC2). The rim is rich in Al (darker, $\text{Cr}\#=3.5$) compared to Cr-rich core ($\text{Cr}\#=4.8$). **h** Back-scattered electron image of a sulphide bleb in Opx in the veinlet of orthopyroxenite (sample BN92). Note cubanite (Cb) exsolutions at the margin areas of Ni-bearing pyrrhotite (Po). The dark areas on the margin of the sulphide grain are Fe–Cu oxides

0.773. The values of $\text{Cr}\# (=100 \times \text{Cr}/[\text{Al} + \text{Cr}])$ range from 7.7 to 18.7 in BNH 5 and from 3.5 to 4.9 in BNC2 (Fig. 4). Furthermore, spinel grains in BNC2 show compositional zoning with rims ($\times 30 \mu\text{m}$) high in Mg and low in Cr (Table 1; Fig. 2g). Spinel contains lower $\text{Cr}\#$ than that of peridotites in the area.

Secondary Opx grains are texturally distinct from the primary Opx because of their shape and abundant fluid inclusions, but their compositions are similar in individual samples, suggesting that equilibration was attained among grains (Table 1). Orthopyroxene does not exhibit compositional zoning in grains (Table 1), which is consistent with equilibration among Opx grains, which have low Cr_2O_3 (0.09–0.48 wt.%) and $\text{Mg}\#$ (84.5–89.2), similar Al_2O_3 (2.87–5.10 wt.%), and high TiO_2 (0.20–0.59 wt.%) compared to Opx in peridotites (Fig. 5).

Amphiboles contain overall high TiO_2 (3.38–4.83 wt.%) and alkalis ($\text{K}_2\text{O} + \text{Na}_2\text{O} = 2.50\text{--}8.93$ wt.%) and low $\text{Mg}\#$ (53.3–71.3). Their compositions suggest that they are sodic–calcic Amp, such as richterite, magnesio-katophorite, and winchite based on the amphibole-classification of Leake et al. (1997), but their phases were not identified due to their large compositional variation within grains and small sizes. The compositional variation suggests that Amp was possibly introduced at a very late stage by reaction between xenoliths and host melt.

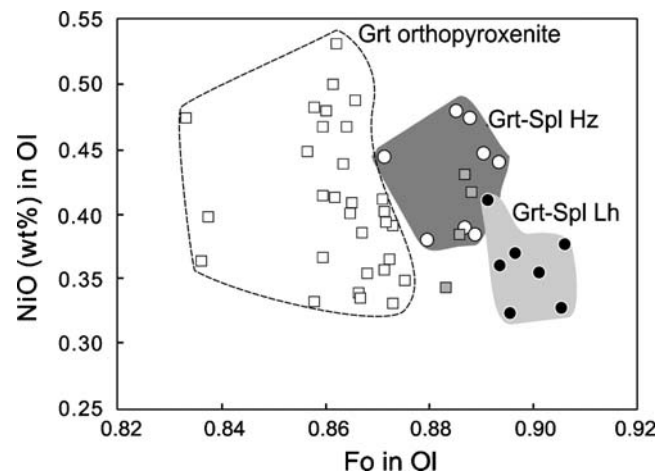


Fig. 3 Plot of NiO (wt.%) in Ol vs. Fo for olivines. Filled circles garnet-spinel lherzolites (Grt–Spl Lh), open circles garnet-spinel harzburgites (Grt–Spl Hz), open squares Grt orthopyroxenites, filled grey squares veinlet of Grt orthopyroxenites

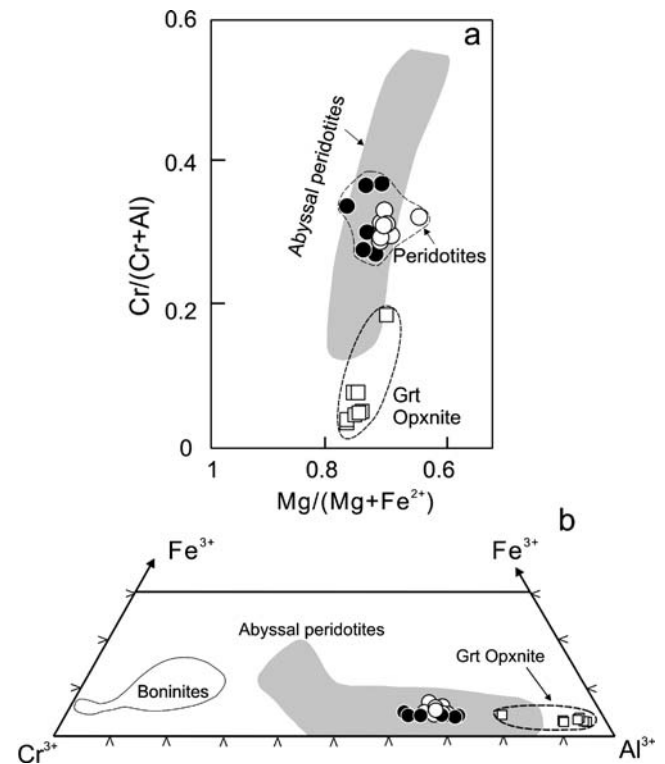


Fig. 4 Binary $[\text{Cr}/(\text{Cr} + \text{Al})$ vs. X_{Mg}] and ternary ($\text{Fe}^{3+}\text{--}\text{Cr}^{3+}\text{--}\text{Al}^{3+}$) diagrams for Cr-spinel in the Grt orthopyroxenites (Grt Opxnite) and other Grt-bearing peridotites xenoliths from Pali Aike. Symbols are the same as in Fig. 3. Each data point represents one grain. Cr-spinel grains are rare in Grt orthopyroxenites and found only in two samples (BNH 5, BNC2). These grains in orthopyroxenites show compositional variations, same as in Fig. 2g, but the differences between cores and rims are too small to be shown in the diagram. Note that these Cr-spinel grains in Grt orthopyroxenites contain low Cr^{3+} and Fe^{3+} . Data sources: abyssal peridotites (Dick and Bullen 1984; Barnes and Roeder 2001), boninite (Barnes and Roeder 2001)

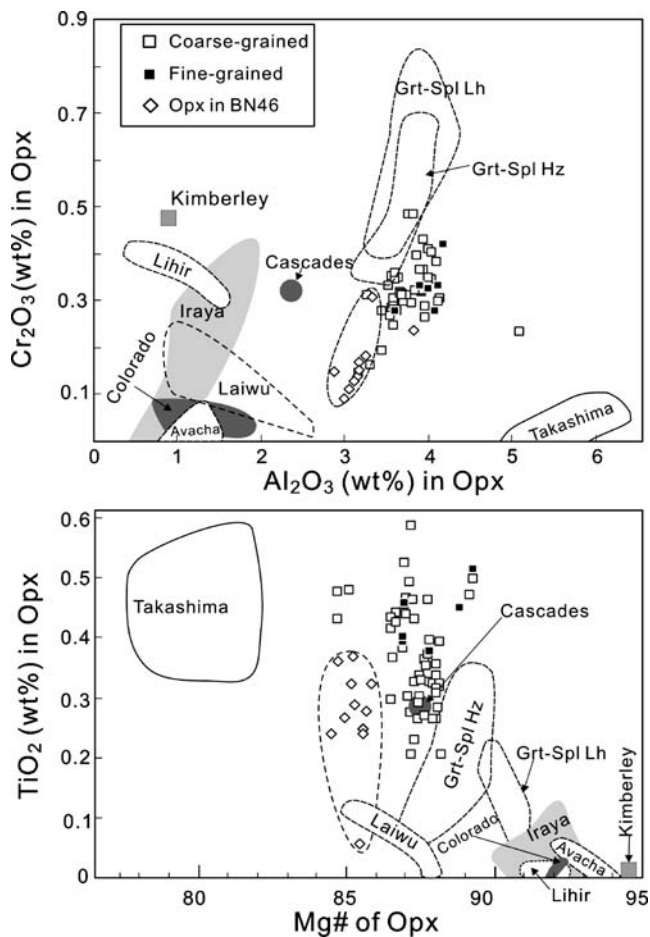


Fig. 5 Relationships between Cr_2O_3 vs. Al_2O_3 and TiO_2 versus $\text{Mg}\#$ of secondary orthopyroxene in peridotites and orthopyroxenites. *Open squares* coarse grains, *filled squares* fine grains, *diamonds* grains in sample BN46. Note that orthopyroxene in Grt orthopyroxenite has a different composition from orthopyroxenes in Grt-bearing peridotites from the area, and secondary orthopyroxenes replacing olivine in mantle wedges. Data source Avacha, Russia (Arai et al. 2003), Iraya, Philippines (Arai et al. 2004), Takashima, Japan (Arai et al. 2006), Cascades, USA (Ertan and Leeman 1996), Colorado Plateau, USA (Smith et al. 1999), Laiwu, China (Chen and Zhou 2005), Kimberley, South America (Bell et al. 2005), and Lihir, Papua New Guinea (McInnes et al. 2001)

Phlogopite is characterized by high TiO_2 (5.18–7.13 wt.%) and $\text{Mg}\#$ ranging from 82.2 to 84.7 (Table 1). The compositions are similar within grains and samples, and their occurrences are spatially associated with Ti–Amp.

Major, minor and platinum-group elements in bulk samples

Garnet orthopyroxenites contain relatively high SiO_2 (48.8–54 wt.%), Al_2O_3 (3.62–11.3 wt.%) and TiO_2 (up to 2.0 wt.%), and low $\text{Mg}\#$ (84.6–88.0) compared to Grt-bearing peridotites in the area ($\text{SiO}_2 < 47$ wt.%; $\text{Al}_2\text{O}_3 < 4$ wt.%; $\text{TiO}_2 < 0.4$ wt.%; $\text{Mg}\# > 87$; Fig. 6), but their compositions are distinctly different from those of

host basalts and websterites in the study area (Fig. 6). Websterite has low total PGE contents and fractionated primitive mantle-normalized PGE patterns (Fig. 7d). The data support the suggestion that websterites are cumulates of melt.

Garnet orthopyroxenites contain high contents of PGE (12.9 to 29.8 ppb in total), comparable to the primitive

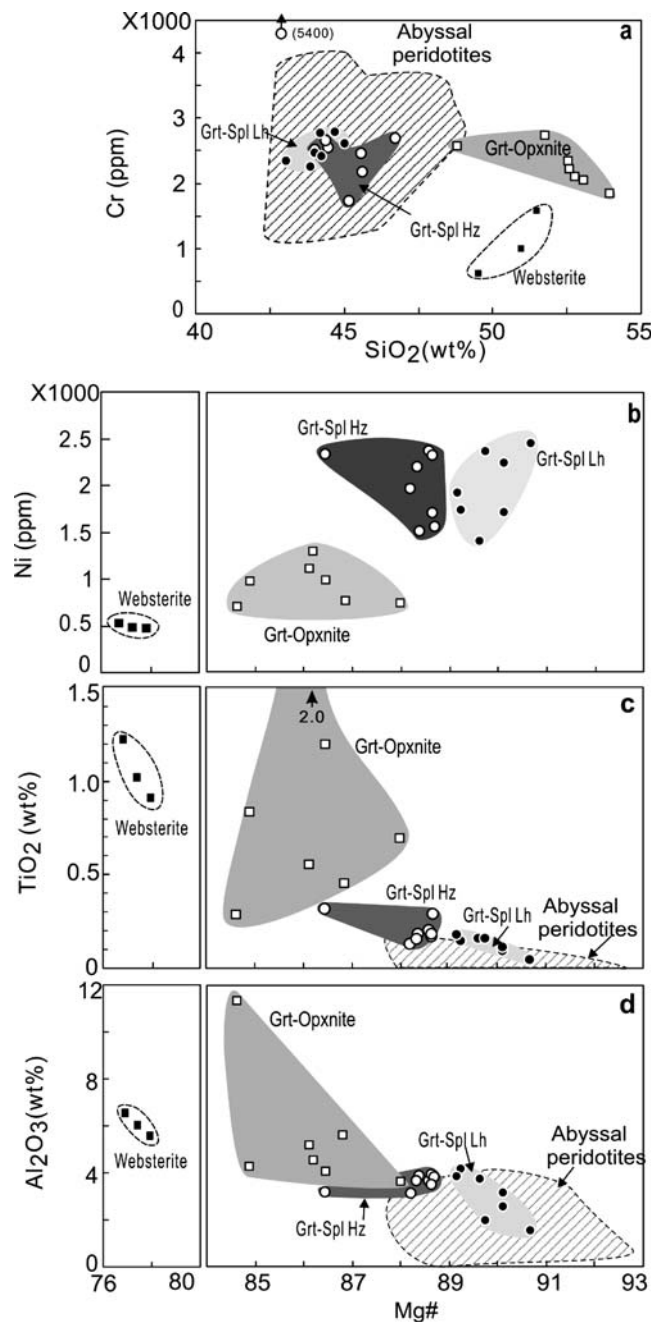
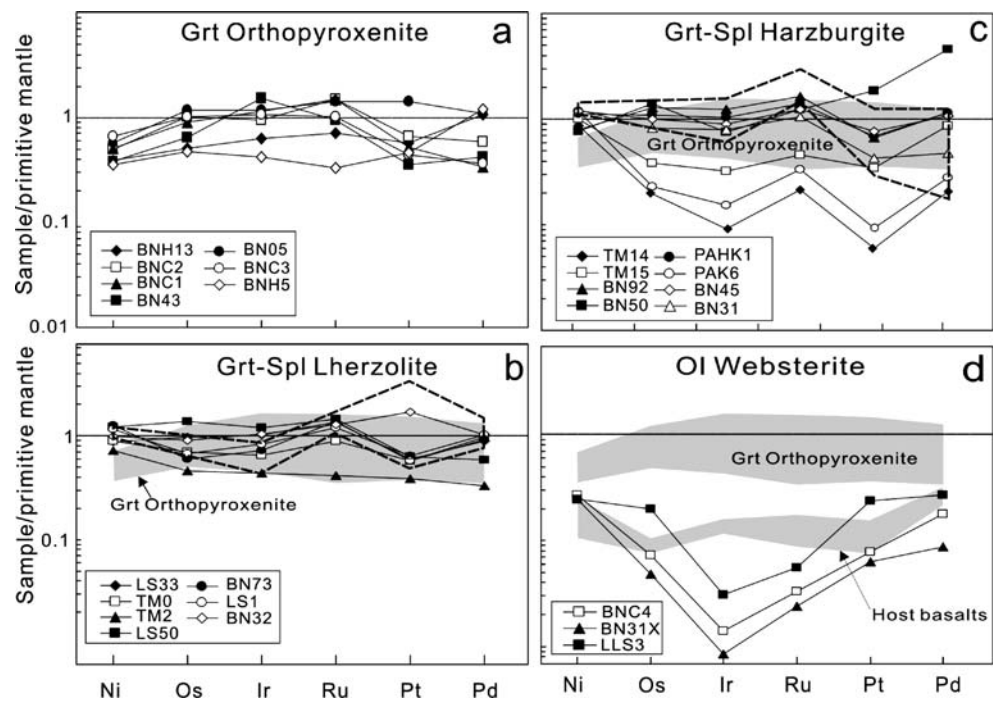


Fig. 6 Bulk chemical compositions of mantle xenoliths from the Pali Aike area. **a** Cr vs. SiO_2 , **b** Ni vs. $\text{Mg}\# (=100 \times \text{Mg} / (\text{Mg} + \text{total Fe}))$, **c** TiO_2 vs. $\text{Mg}\#$, and **d** Al_2O_3 vs. $\text{Mg}\#$. *Oblique hatched areas* are abyssal peridotites (Niu 2004). *Filled squares* websterite, *other symbols* are the same as in Fig. 3

Fig. 7 Primitive mantle-normalized platinum-group elements of mantle xenoliths. **a** Grt orthopyroxenite, **b** Grt–Spl lherzolite, **c** Grt–Spl harzburgite, and **d** Ol websterite. Note that shaded area in **b** and **c** is the field of Grt orthopyroxenite, and that shaded areas in **d** are the fields for Grt orthopyroxenites and host basalts. The data of peridotites from Ronda and Beni Bousera are from Gueddari et al. (1996). Primitive mantle values are from McDonough and Sun (1995)



mantle values, and they have nearly flat primitive mantle-normalized PGE patterns (Fig. 7). In terms of absolute and relative PGE abundances, the Grt orthopyroxenites are comparable to Grt-bearing peridotites in the study area (Fig. 7; Table 2). Furthermore, the data from orthopyroxenites are similar to mantle peridotites from many other areas, such as Ronda in Spain and Beni Bousera in Morocco (e.g., Gueddari et al. 1996).

Orthopyroxenites contain higher concentrations of S (10–140 ppm) compared to Grt–Spl harzburgites (5–25 ppm; Table 2; Fig. 8a). Garnet–Spl lherzolites contain slightly higher S (10–50 ppm) compared to the Grt–Spl harzburgites (Fig. 8a). Their lower concentrations in harzburgites are consistent with their incorporation into melt during partial melting.

Estimates of temperature and pressure

Samples that contain garnet grains equilibrated with other minerals (Opx, Cpx and Ol) were selected for temperature and pressure estimates. Temperatures for garnet orthopyroxenite xenoliths were determined using two-pyroxene thermometers (Wells 1977; Brey and Köhler 1990) and Ca-in-Opx thermometry (Brey and Köhler 1990). The two-pyroxene thermometry of Brey and Köhler (1990) yielded systematically higher temperatures by up to ~100°C than the results using the Wells' thermometry (Table 3). The Ca-in-Opx thermometry (Brey and Köhler 1990) gave roughly similar temperatures, with the differences <80°C, as the two-pyroxene thermometry of Wells (1977; Table 3).

Pressures were estimated using the temperature results of Wells (1977). For sample BNO5 without clinopyroxene, the pressure was calculated based on the temperature using the Ca-in-Opx thermometry. The Al-in-Opx barometry of Brey and Köhler (1990) yielded systematically higher pressures up to ~2 kb than that of Nickel and Green (1985; Table 3). The calculated pressures for garnet orthopyroxenites are comparable with or slightly higher than those Grt-bearing peridotite xenoliths in the area (Kempton et al. 1999a; Wang, 2007).

Discussion

Relationships between peridotites and orthopyroxenites

Based on the texture of Opx replacing Ol and Cpx described in the previous sections, the original rocks were either harzburgites or lherzolites and were subsequently metasomatized to form orthopyroxenites. This metasomatic origin of orthopyroxenite is further supported by the finding of a high Mg Ol (Fo=90.4) inclusion in Opx. The Mg content of this olivine is similar to that of peridotites and this Ol grain, which is totally enclosed by a coarse-grained Opx, apparently escaped equilibration with Ol outside the Opx. A metasomatic origin is also supported by high concentrations of refractory elements, such as Ni, Cr and Ir-type PGE. Cumulates should contain low Ir-type PGE, such as determined for the websterites, and high ratios of Pt-type PGE/Ir-type PGE compared to mantle residues, because refractory Ir-type PGE remain in mantle residue during

Table 2 Major and selected trace element abundances of selected samples of Grt orthopyroxenites, websterites and host basalts

Sample	Grt orthopyroxenite						Websterite			Basalt		
	BN43	BNC1	BNC2	BNC3	BNO5	BNH5	BNH13	BNC4	BN31x	LLS3	LLS-1(v)	TM-15(v)
Major elements (wt.%)												
SiO ₂	53.95	52.76	53.02	51.74	52.53	48.80	52.58	49.51	50.95	51.47	44.59	41.72
TiO ₂	0.70	1.20	0.84	2.00	0.55	0.29	0.46	1.21	1.02	0.91	3.46	2.60
Al ₂ O ₃	3.62	4.05	4.28	4.57	5.22	11.34	5.65	6.54	6.00	5.58	11.32	9.06
Fe ₂ O ₃ (t) ^a	8.64	9.53	10.56	9.74	9.69	9.66	9.07	9.76	10.07	10.68	13.29	12.63
MnO	0.12	0.11	0.13	0.12	0.13	0.19	0.14	0.14	0.15	0.15	0.17	0.18
MgO	31.93	30.71	29.93	30.68	30.34	26.80	30.24	16.40	17.46	19.08	10.85	17.10
CaO	0.91	0.93	0.92	0.78	1.04	2.19	1.54	13.71	12.59	10.48	8.74	9.06
Na ₂ O	<0.05	<0.05	<0.05	<0.05	<0.05	<0.05	<0.05	1.61	1.47	1.30	3.05	2.96
K ₂ O	0.02	0.02	0.14	0.03	0.02	0.01	0.27	0.07	0.01	0.00	1.95	1.66
P ₂ O ₅	0.02	0.02	0.02	0.02	0.01	0.05	0.03	0.05	0.02	0.03	0.75	0.99
Total	100.1	99.64	100.2	100.0	99.87	99.61	100.2	99.19	99.94	99.94	98.44	98.31
Mg# ^b	0.880	0.865	0.849	0.862	0.861	0.846	0.868	0.769	0.775	0.780	0.618	0.728
Trace elements in ppm												
Cr	1,843	2,125	2,061	2,735	2,348	2,576	2,215	609	1,002	1,576	313	650
Ni	743	991	971	1,292	1,114	698	761	528	481	480	204	497
S	10.12	22.10	11.53	15.19	17.41	138.1	144.0	34.84	23.97	89.47	nd	nd
Platinum-group elements in ppb												
Os	2.30	3.17	3.62	3.57	4.17	1.69	1.79	0.26	0.17	0.71	0.27	0.37
Ir	4.99	3.78	3.07	3.53	3.81	1.37	2.07	0.05	0.03	0.10	0.38	0.52
Ru	4.82	7.61	7.59	5.23	7.22	1.70	3.63	0.17	0.12	0.29	0.45	0.88
Pt	2.60	3.77	4.78	3.25	10.25	3.41	4.13	0.57	0.46	1.75	0.55	1.13
Pd	1.68	1.36	2.35	1.44	4.31	4.76	4.22	0.71	0.35	1.07	0.86	1.27
Ru/Ir	0.97	2.01	2.47	1.48	1.89	1.24	1.76	3.75	4.44	2.85	1.18	1.69
Pd/Ir	0.34	0.36	0.77	0.41	1.13	3.49	2.04	15.57	12.59	10.60	2.25	2.45
(Pt + Pd)/ (Os + Ir)	0.59	0.74	1.07	0.66	1.83	2.67	2.17	4.19	4.10	3.49	2.17	2.70
PGE-total	16.38	19.69	21.41	17.01	29.76	12.92	15.84	1.76	1.14	3.92	2.51	4.18

nd not determined

^aTotal Fe as Fe₂O₃

^bMg# = 100 × Mg / (Mg + ΣFe)

partial melting (e.g., Brenan et al. 2005). Nickel and Cr are also highly compatible and remain in the residual peridotites during partial melting. In contrast, websterite cumulates in our samples contain significantly lower Ni (<530 ppm) and Cr (<1,600 ppm) and higher ratios of Pt-type PGE/Ir-type PGE, ~4 (Table 2). Similar Cr and PGE contents and unfractionated PGE patterns of orthopyroxenites and peridotites suggest that the orthopyroxenites are unlikely to be cumulates, but rather formed from Grt-bearing peridotites by metasomatism.

Nature of metasomatizing agent

Garnet orthopyroxenites contain higher SiO₂, Al₂O₃, TiO₂, and lower Mg# in bulk rocks compared to Grt-bearing peridotites in the area (Table 2; Fig. 6), suggesting that the metasomatizing agent is likely to be rich in Si, Al, Ti and Fe. Therefore, the metasomatizing agent is most likely melt

rather than fluid because Ti and Al are relatively immobile in aqueous fluids. The proposed interpretation is supported by high F/Cl ratios in Ti-phlogopite and Ti-Amp in our samples (Table 1), because F is preferentially retained in melt (e.g., Willmore et al. 2000). High Ti in the metasomatizing melt is supported by high Ti contents in secondary Opx, as well as in phlogopite and Amp, whereas high Al contents in melt are reflected in the rims of individual spinel grains (Table 1). Furthermore, the common existence of Ti-phlogopite and Ti-Amp and high alkali contents (K₂O+Na₂O, up to 9 wt.%) in Amp suggest that the melt was also rich in alkalis.

The low Mg# values of secondary Opx likely reflect the character of the metasomatizing melt (Wang et al. 2007). The olivine in the metasomatic orthopyroxenites is much more Fe rich than olivine in typical residual upper mantle peridotites, and so the melt that formed the olivine must have been evolved compared to melt in equilibrium

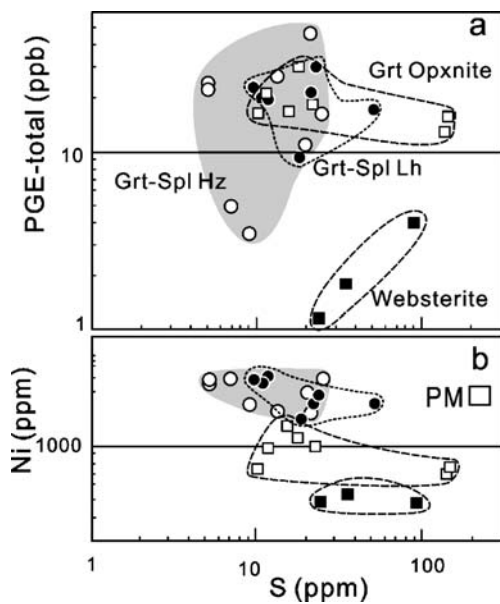


Fig. 8 Plot of **a** PGE-total vs. S, and **b** Ni vs. S. Filled square websterite, other symbols are the same as in Fig. 3. Primitive mantle values are from McDonough and Sun (1995). Data for Grt–Spl Lh and Grt–Spl Hz are from Wang (2007)

with primitive mantle ($Mg\# \sim 89$) or residual mantle olivine ($Mg\# > 89$). The $Mg\#$ of the metasomatizing melt was roughly evaluated using the composition of Ol. Olivine is a relict phase but it equilibrated with Opx in orthopyroxenites, based on the positive correlation of $Mg\#$ between Ol and Opx. The Fe–Mg exchange coefficient, K_d , between Ol and melt is a function of temperature, pressure, and compositions of Ol and the melt (Toplis 2005). The effect of pressure on K_d is small (~ 0.01 per GPa). However, the concentrations of Si and alkalis of the melt and the temperature may affect K_d under high pressures. High degrees of partial melting occur at high temperatures (increasing K_d), but such melt is generally lower in Si (lowering K_d); these effects cancel each other, resulting in a K_d value close to 0.3, which is commonly observed in natural systems (Roeder and Emslie

1970). Considering the above factors, we used a K_d value of 0.3 for calculation. The calculated $Mg\#$ of the melt is 56.0–63.7.

The evolved nature of the metasomatizing melt explains the variable and low Cr# of spinel (3.5–1.9) in orthopyroxenites. The Cr content of a melt decreases quickly during solidification of the melt, and the spinel formed during such crystallization shows a highly variable Cr# (Barnes and Roeder 2001). The preservation of a compositional variation in spinel grains in our samples suggests that orthopyroxenites were brought to the surface not long after metasomatism, since spinel easily equilibrates with melt at high temperatures (e.g., Hammond and Taylor 1982).

Origin of metasomatizing melt

There are two possible origins of the metasomatizing melt that we argue was responsible for the formation of the orthopyroxenites: (1) a slab-melt and/or arc-related magma, and (2) melt unrelated to subduction. The first possibility is rejected because slab-melt and arc magmas contain low Ti (e.g., Prouteau et al. 1999), whereas the melt responsible for the formation of Grt orthopyroxenite was rich in Ti. In addition, the Pali Aike area is over 100 km far from an identified arc volcano (Fig. 1). Furthermore, the Al_2O_3 content in secondary Opx in our samples is high (2.87–5.10 wt.%), whereas secondary Opx formed in subarc mantle peridotites has a low Al_2O_3 content (< 2 wt.% in most cases; Fig. 5; Arai et al. 2003, 2004), and the pyroxenites at the base of arc section also show low Al contents as shown at the Talkeetna arc along the crust–mantle boundary in south central Alaska (DeBari and Coleman 1989; DeBari and Sleep 1991). Instead, we suggest that the metasomatizing melt for formation of Grt orthopyroxenite in Pali Aike was an alkali basaltic melt that originated from asthenospheric mantle, because such a melt is commonly high in Ti (Gibson et al. 1995), as are the Pali Aike alkali basalts (Skewes and Stern 1979). Second, Sr and Nd isotopic data for modally

Table 3 Temperature and pressure estimates for the garnet-bearing orthopyroxenite xenoliths from Pali Aike area

Sample	Rock type	Temperature (°C)			Pressure (kbar)	
		Wells (77) ^a	B&K-2Px (90) ^b	B&K-Ca (90) ^c	B&K Al-in Opx (90) ^d	N&G Al-in Opx (85) ^e
BN05	Grt Orthopyroxenite			1,024	22.8	20.9
BN92		988	1,077	1,014	22.5	20.6
BNH13		1,069	1,150	1,005	26.5	24.6
BN46		984	1,079	1,033	22.9	21.6
BNH5		1,064	1,170	984	26.1	24.8

^a Wells (1977) two-pyroxene thermometer

^b Brey and Köhler (1990) two-pyroxene thermometer

^c Brey and Köhler (1990) Ca-in-Opx thermometer

^d Brey and Köhler (1990) Al-in-Opx barometer

^e Nickel and Green (1985) Al-in-Opx barometer

metasomatized Grt-bearing harzburgites (Kempton et al. 1999b; Stern et al. 1999) are similar to the Pali Aike host basalts (Stern et al. 1990) and other Patagonian Quaternary alkali basalts, which show trace element patterns similar to oceanic island basalts and have a well-established asthenospheric origin (Gorring et al. 1997). The subduction of the Chile ridge since the mid-Miocene (~14 Ma) resulted in the formation of a slab window which allowed upwelling of asthenospheric melt to form the voluminous plateau basalts (Gorring et al. 1997).

Our xenolith samples are hosted by olivine alkali basalts that are rich in Ti and alkalis; therefore, the host basalt is potentially responsible for the metasomatizing event. However, we discount this possibility because many host basalts are silica-unsaturated and contain normative nepheline (D'Orazio et al. 2000). They are primitive in composition, with high contents of MgO, Ni and Cr up to 17.1 wt.%, 650 and 500 ppm, and relatively low contents of SiO₂, <45 wt.% (Table 2), even lower than peridotites. To enrich the peridotites with Si, an evolved melt is required. Therefore, we consider that the metasomatizing melt has the same affinity as and is co-genetic with the host alkali basalt, but the two are different.

A Si-poor alkali melt may evolve to become a Si-saturated magma. Some plateau basalts in Pali Aike contain Ol and normative hypersthene (D'Orazio et al. 2000). The existence of these minerals indicates that the composition of the parental magmas plots in the inner tetrahedron of Ol–diopside–enstatite–albite in the system of nepheline–diopside–quartz–Ol (Yoder and Tilley 1962). At great depths, Ol and diopside would crystallize from the magmas without plagioclase because plagioclase is not stable under high pressures. The fractional crystallization of Ol and diopside results in the composition of the residual melt migrating towards the quartz apex, causing an enrichment of Si. The evolved Si-rich melt is not in equilibrium with mantle Ol and Cpx and therefore, it is not surprising to observe Si-saturated melt replacing Ol and Cpx during its infiltration through mantle peridotites to form secondary Opx. A similar process of replacement of Ol by Opx was proposed by Arai et al. (2006) in explaining the generation of the Si-saturated evolved alkali basalts that were responsible for Fe-rich orthopyroxenite xenoliths in Takashima, southwestern Japan.

Formation of Grt orthopyroxenites in the Pali Aike area

Textural evidence suggests that secondary Opx in our samples formed mostly at the expense of Ol via the reaction:



The secondary Opx contains more Fe, Si, Ti, and Al than Ol, and these components were supplied from the melt. Therefore, the protolith of orthopyroxenites is most likely Grt-bearing harzburgites.

This proposed interpretation is consistent with microscopic textural evidence from the orthopyroxenites. They commonly contain small irregularly shaped fragments of harzburgites, which most likely represent a remnant of the original harzburgites.

Orthopyroxenite samples BNH5 and BNH13 contain relatively high CaO (2.19 and 1.54 wt.%, respectively) and relict Cpx and Ol in secondary Opx; the secondary Opx is commonly associated with Ti–Amp. These orthopyroxenites likely formed from Grt-bearing lherzolites. In addition to reaction (1), Cpx in these samples also reacted with the metasomatizing melt, forming Opx:



BN46 contains relict grains of Cpx associated with secondary Opx, but the Opx contains distinctly lower Cr contents (~0.15 wt.%) and Mg# (~85) than in other samples (Table 1; Fig. 5). Therefore, BN46 is most likely a metasomatic product of cumulate websterites. Unfortunately, the sample was barely sufficient for thin-section observation and too small to obtain a bulk-rock composition to verify our interpretation.

The values for temperature and pressure of the last equilibrated Grt orthopyroxenites (Table 3) are similar to those of garnet-bearing lherzolites and harzburgites in the area (Kempton et al. 1999a; Wang 2007), suggesting that these Grt orthopyroxenites formed at the same P and T conditions as those wall rock peridotites before being entrained by the host Pali Aike basalts.

Behavior of Cr, Ni, S, PGE and other elements during the formation of Grt orthopyroxenites

Pali Aike orthopyroxenite samples show an enrichment of alkalis, Si, Al, Ti, Fe, and H₂O, a minor depletion of Ni, and no change in content of Cr and PGE (due to an essential immobility during metasomatism). The enrichment of Si and Al, based on bulk-rock compositions (Fig. 6), is reflected by an increased modal abundance of Opx, whereas the enrichment of Ti and Fe is well illustrated by the mineral compositions, since the metasomatic products contain high Ti and Fe, and the rims of relict Cpx are enriched in Ti.

Nickel contents in bulk rock of orthopyroxenites are slightly lower than those of peridotites (Figs. 6b, 8b; Table 2), but NiO contents in Ol in orthopyroxenites are

higher, ranging from 0.33 to 0.53 wt.% (Fig. 3), than those peridotites. High NiO contents in Ol in orthopyroxenites are explained by the low modal abundance of Ol and the high distribution coefficient of Ni between Ol and Opx (Kennedy et al. 1993; Kelemen et al. 1998). During metasomatism, the volume of Ol decreased (<1 vol.%), which resulted in high Ni contents in the remaining Ol. Nickel is also present in sulphides and the amounts of Ni hosted by sulphides are evaluated using Ni/S of sulphides and the contents of S in bulk rocks. Electron probe analyses show the atomic ratios of Ni/S in sulphides vary from 0.07 to 0.6 with median value at 0.2, and the bulk S contents vary from 10 to 144 ppm (Table 2). The maximum amount of Ni hosted by sulphides is 158 ppm. The content is far less than the Ni contents in bulk rocks (700–1,290 ppm; Table 2). Therefore, the majority of Ni in the rocks is hosted by silicate minerals, such as Opx and Ol. The minor role of sulphides as the host of Ni is consistent with the lack of a positive correlation between S and Ni (Fig. 8b).

The concentrations of PGE and their primitive mantle-normalized patterns of PGE for orthopyroxenites are similar to those of anhydrous Grt–Spl lherzolite samples (e.g., BN73 and LS1) and other metasomatized Grt-bearing samples (Fig. 7). Furthermore, the PGE abundance and patterns are also comparable with mantle peridotites in other areas, e.g. lherzolitic massifs from Ronda and Beni Bousera (Gueddari et al. 1996; Fig. 7b, c). The data suggest that metasomatism did not greatly modify the abundance of PGE, particularly Ir-type PGE. Palladium shows minor scatter in its concentrations in several samples (Fig. 7), consistent with the high mobility of PGE in aqueous fluids (e.g., Hinchey and Hattori 2005). The immobility of Ir-type PGE suggests that they are useful to evaluate the protoliths of metasomatized ultramafic rocks.

In mantle peridotites, sulphides are considered to be the host of PGE (e.g., Hart and Ravizza 1996) because of the extremely high partition coefficients, >1,000, for PGE between sulphide and silicate melt (e.g., Crocket et al. 1997; Fleet et al. 1996). This interpretation is not applicable to our rocks because several Grt-bearing peridotite samples (i.e. LS50, PAHK1 and BN45) contain very low contents of S (<10 ppm), yet high total PGE (>20 ppb; Fig. 8a), and PGE contents are independent of S. For example, samples BNH13 and BNH5 contain high S (144 and 138 ppm S, respectively) yet are relatively low in total PGE, 15.8 and 12.9 ppb, respectively, compared with the PGE content of other low S samples. This is also supported by the higher sulphide modal abundance in orthopyroxenites (more than 20 grains per section) than in those peridotites (three to five grains per section). Therefore, the PGE may occur (a) in platinum group minerals (PGM), such as Ru–Os±Ir

sulfides and Pt–Ir±Os alloys (Ahmed and Arai 2002; Ahmed et al. 2006; Luguët et al. 2007), and/or (b) in silicate and oxide minerals.

Comparison with orthopyroxenites in other regions

Peridotites in subarc mantle are refractory due to high degrees of partial melting; Ol in such refractory peridotites contains low Al and high Mg, Fo>90. Slab-derived melt and aqueous fluids are generally high in Si and low in Cr and Ti. Therefore, secondary Opx formed from Ol by reacting with a slab-derived fluid/melt usually contains low contents of Al₂O₃ (<2 wt.%), TiO₂ (<0.1 wt.%) and Cr₂O₃ (<0.4 wt.%), and has a high Mg# (90–94), as documented in the Colorado Plateau (Smith and Riter 1997; Smith et al. 1999), Avacha in Russia (Arai et al. 2003) and Iraya in the Philippines (Arai et al. 2004; Fig. 5). Secondary Opx in a phlogopite-bearing orthopyroxenite (Ertan and Leeman 1996) from the cascades has a lower Mg#, ~87, comparable to our Opx, but still contains low TiO₂ (~0.06 wt.%) and moderate Al₂O₃ (~2.36 wt.%); the composition is also similar to that of secondary Opx in mantle wedges (Fig. 5).

Converting Ol to Opx through metasomatism by a Si-rich melt and/or fluid is also reported in SCLM beneath ancient cratons, such as North China craton which lost its Archean keel in the Phanerozoic (Chen and Zhou 2005; Liu et al. 2005; Malaspina et al. 2006) and Kaapvaal craton, South Africa (Kesson and Ringwood 1989; Kelemen et al. 1998; Bell et al. 2005). Secondary Opx formed in these SCLM show low contents of Ti, Cr, Al, and high Mg# similar to subarc mantles. For example, secondary Opx in orthopyroxenite from Kimberley, South Africa from SCLM beneath Kaapvaal craton contains low TiO₂ (<0.01 wt.%), Cr₂O₃ (~0.48 wt.%), Al₂O₃ (~0.88 wt.%), and high Mg# (~95; Fig. 5; Bell et al. 2005). Similarly, secondary Opx in orthopyroxenites from Laiwu from SCLM beneath North China craton shows low TiO₂ (<0.11), Cr₂O₃ (<0.31 wt.%), Al₂O₃ (1–2.6 wt.%), and intermediate Mg# (85–88; Fig. 5; Chen and Zhou 2005). In both cases, the orthopyroxenites were considered to be formed from harzburgites by reaction with a melt derived from an old subducted oceanic lithosphere (Bell et al. 2005; Chen and Zhou 2005). The interpretation is consistent with hypothesis that craton and underlying SCLM maybe formed from ancient refractory wedge mantle (Parman et al. 2004).

Secondary Opx from Takashima is interpreted to be formed from peridotites through reaction with an evolved alkali basaltic melt (Arai et al. 2006). The participation of such melt is suggested from the high contents of TiO₂ (0.37–0.57 wt.%) and Al₂O₃ (5–6 wt.%), and the low Mg# (73–88) and Cr₂O₃ (<0.08 wt.%) in Opx (Fig. 5).

Pali Aike Opx contains relatively high Mg# and low Cr₂O₃, similar to that expected for secondary Opx formed during reaction with slab-derived fluid and/or melt (Fig. 5), but our Opx contains high Ti and Al. The latter feature is similar to Opx formed during the reaction with evolved alkali melt in Takashima.

Peridotites in SCLM in continental rifts and hotspot areas are commonly affected by the upwelling asthenospheric mantle melt. In these tectonic settings, alkali basaltic melt commonly ascended from the asthenospheric mantle to the overlying SCLM. Pervasive infiltration of melt may have resulted in the formation of orthopyroxenites at depth in the SCLM if this melt experienced the similar evolution process as discussed in this study, and these orthopyroxenites may resemble our samples.

Conclusions

Garnet orthopyroxenite xenoliths are common in the Quaternary Pali Aike volcanic rocks, and contain minor Ti-rich Amp and phlogopite, and abundant relict Ol grains in Opx. The xenoliths were likely produced from Grt-bearing harzburgites during metasomatic replacement of Ol by Opx during reaction with a Ti-rich alkali melt. Injection of the melt also produced veinlets of Grt-bearing orthopyroxenite with diffuse boundaries in harzburgite xenoliths.

The Opx in Grt orthopyroxenites contains relatively high TiO₂ (0.20–0.59 wt.%), moderate Al₂O₃ (3.27–5.10 wt.%) and Cr₂O₃ (0.15–0.48 wt.%), and low MgO (Mg#=85–88) compared to Grt-bearing peridotites. The compositions are distinctly different from secondary Opx formed from Ol through reaction with slab-fluid and/or melt that was generated in mantle wedges. The metasomatizing agent is most likely an evolved alkali melt, genetically related to the Pali Aike alkali basalts, that was derived from the underlying asthenospheric mantle.

The orthopyroxenites contain high concentrations of Cr, Ni, and PGE comparable to peridotites, suggesting that these elements were essentially immobile during metasomatism by the evolved asthenospheric melt. The contents of PGE are independent of S and they are most likely present in PGM, silicate and oxide minerals.

Acknowledgement This work was financially supported by a NSERC Discovery Grant to KHH and an Ontario Graduate Scholarship in Science and Technology and the University of Ottawa Excellence Scholarship to JW. We thank P. Kelemen for review of an earlier draft of the manuscript and constructive suggestions. We also thank M. Wilk-Aleman for help of PGE analyses, R. Hartree for XRF analysis, and G. Mrazek for the preparation of sections. Thanks are also given to P. Jones at Carleton University for his help with the electron microprobe analyses, and M.A. Skewes who collaborated in the collection of the samples. The manuscript benefited from the constructive comments by M. D'Orazio and an anonymous journal reviewer.

References

- Ahmed AH, Arai S (2002) Unexpectedly high-PGE chromitite from the deeper mantle section of the northern Oman Ophiolite and its tectonic implications. *Contrib Mineral Petrol* 143:263–278
- Ahmed AH, Hanghøj K, Kelemen PB, Hart SR, Arai S (2006) Osmium isotope systematics of the Proterozoic and Phanerozoic ophiolitic chromitites; in situ ion probe analysis of primary Os-rich PGM. *Earth Planet Sci Lett* 245:777–791
- Arai S, Kida M (2000) Origin of fine-grained peridotite xenoliths from Iraya volcano of Batan Island, Philippines: deserpentinization or metasomatism at the wedge mantle beneath an incipient arc. *Island Arc* 9:458–471
- Arai S, Ishimaru S, Okrugin VM (2003) Metasomatized harzburgite xenoliths from Avacha volcano as fragments of mantle wedge of the Kamchatka arc: an implication for the metasomatic agent. *Island Arc* 12:233–246
- Arai S, Takada S, Michibayashi K, Kida M (2004) Petrology of peridotite xenoliths from Iraya Volcano, Philippines, and its implication for dynamic mantle-wedge processes. *J Petrol* 45:369–389
- Arai S, Shimizu Y, Morishita T, Ishida Y (2006) A new type of orthopyroxenite xenolith from Takashima, Southwest Japan: silica enrichment of the mantle by evolved alkali basalt. *Contrib Mineral Petrol* 152:387–398
- Arth J, Hanson G (1975) Geochemistry and origin of early Precambrian crust of northwestern Minnesota. *Geochim Cosmochim Acta* 39:325–362
- Barnes SJ, Roeder PL (2001) The range of spinel compositions in terrestrial mafic and ultramafic rocks. *J Petrol* 42:2279–2302
- Bell DR, Gregoire M, Grove TL, Chatterjee N, Carlson RW, Buseck PR (2005) Silica and volatile-element metasomatism of Archean mantle: a xenolith-scale example from the Kaapvaal Craton. *Contrib Mineral Petrol* 150:251–267
- Brey GP, Köhler T (1990) Geothermobarometry in four-phase lherzolites: II. New thermobarometers, and practical assessment of existing thermobarometers. *J Petrol* 31:1353–1378
- Brenan JM, McDonough WF, Ash R (2005) An experimental study of the solubility and partitioning of iridium, osmium and gold between olivine and silicate melt. *Earth Planet Sci Lett* 237:855–872
- Cande SC, Leslie RB (1986) Late Cenozoic tectonics of the southern Chile Trench. *J Geophys Res* 91:471–496
- Chen LH, Zhou XH (2005) Subduction-related metasomatism in the thinning lithosphere: Evidence from a composite dunite-orthopyroxenite xenolith entrained in Mesozoic Laiwu high-Mg diorite, North China Craton. *Geochim Geophys Geosyst* 6: Q06008 doi:10.1029/2005GC000938
- Crocket JH, Fleet ME, Stone WE (1997) Implications of composition for experimental partitioning of platinum-group elements and gold between sulfide liquid and basalt melt: the significance of nickel content. *Geochim Cosmochim Acta* 61:4139–4149
- DeBari SM, Coleman RG (1989) Examination of the deep levels of an island arc: evidence from the Tonsina ultramafic-mafic assemblage, Tonsina, Alaska. *J Geophys Res* 94:4373–4391
- DeBari SM, Sleep NH (1991) High-Mg, low Al bulk composition of the Talkeetna island arc, Alaska; implications for primary magmas and the nature of arc crust. *Geol Soc Am Bull* 103:37–47
- Dick HJB, Bullen T (1984) Chromian spinel as a petrogenetic indicator in abyssal and alpine-type peridotites and spatially associated lavas. *Contrib Mineral Petrol* 86:54–76
- D'Orazio M, Agostini S, Mazzarini F, Innocenti F, Manetti P, Haller MJ, Lashen A (2000) The Pali Aike Volcanic Field, Patagonia: slab-window magmatism near the tip of South America. *Tectonophysics* 321:407–427

- Ertan IE, Leeman WP (1996) Metasomatism of Cascades subarc mantle: evidence from a rare phlogopite orthopyroxenite xenolith. *Geology* 24:451–454
- Fleet ME, Crocket JH, Stone WE (1996) Partitioning of platinum-group elements (Os, Ir, Ru, Pt, Pd) and gold between sulfide liquid and basalt melt. *Geochim Cosmochim Acta* 60:2397–2412
- Francis RD (1990) Sulfide globules in mid-ocean ridge basalts (MORB), and the effect of oxygen abundance in Fe–S–O liquids on the ability of those liquids to partition metals from MORB and komatiite magmas. *Chem Geol* 85:199–213
- Gaetani GA, Grove TL (1997) Partitioning of moderately siderophile elements among olivine, silicate melt, and sulfide melt; constraints on core formation in the Earth and Mars. *Geochim Cosmochim Acta* 61:1829–1846
- Gao S, Rudnick RL, Yuan HL, Liu YS, Xu WL, Ling WL, Ayers J, Wang XC, Wang QH (2004) Recycling lower continental crust in the North China craton. *Nature* 432:892–897
- Gibson SA, Thompson RN, Dickin AP, Leonardos OH (1995) High-Ti and low-Ti mafic potassic magmas: key to plume-lithosphere interactions and continental flood-basalt genesis. *Earth Planet Sci Lett* 136:149–165
- Gorring ML, Kays SM (2001) Mantle processes and sources of Neogene slab window magmas from Southern Patagonia, Argentina. *J Petrol* 42:1067–1094
- Gorring ML, Kays SM, Zeitler PK, Ramos VA, Rubiolo D, Fernandez MI, Panza JL (1997) Neogene Patagonian plateau lavas: continental magmas associated with ridge collision at the Chile triple junction. *Tectonics* 16:1–17
- Gueddari K, Piboule M, Amossé J (1996) Differentiation of platinum-group elements (PGE) and of gold during partial melting of peridotites in the lherzolitic massifs of the Bético–Rifean range (Ronda and Beni Bousera). *Chem Geol* 134:181–197
- Hart SR, Ravizza G (1996) Os partitioning between phases in lherzolite and basalt. In: Basu A, Hart SR (Eds) *Earth processes: reading the isotopic code*. Am Geophys Union Geophys Monogr 95:123–134
- Hammond PA, Taylor LA (1982) The ilmenite/titano-magnetite assemblage: kinetics of re-equilibration. *Earth Planet Sci Lett* 61:143–150
- Hattori KH, Arai S, Clarke DB (2002) Selenium, tellurium, arsenic and antimony contents of primary mantle sulfides. *Can Mineral* 40:637–650
- Hinchey JG, Hattori KH (2005) Magmatic mineralization and hydrothermal enrichment of the High Grade Zone at Las des Iles palladium mine, northern Ontario, Canada. *Miner Depos* 40:13–23
- Kelemen PB (1986) Assimilation of ultramafic rock in subduction-related magmatic arcs. *J Geol* 94:829–843
- Kelemen PB (1990) Reaction between ultramafic rock and fractionating basaltic magma I. Phase relations, the origin of calc-alkaline magma series, and the formation of discordant dunite. *J Petrol* 31:51–98
- Kelemen PB, Hart SR, Bernstein S (1998) Silica enrichment in the continental upper mantle via melt/rock reaction. *Earth Planet Sci Lett* 164:387–406
- Kempton PD, Lopez-Escobar L, Hawkesworth CJ, Pearson DG, Wright DW, Ware AJ (1999a) Spinel±garnet lherzolite xenoliths from Pali Aike; Part 1. Petrography, mineral chemistry and geothermobarometry. In: Gurney JJ, Pascoe MD, Richardson SH (eds) *The JB Dawson volume*. Proceedings of International Kimberlite Conference 7, vol. 1, pp 403–414
- Kempton PD, Hawkesworth CJ, Lopez-Escobar L, Pearson DG, Ware AJ (1999b) Spinel±garnet lherzolite xenoliths from Pali Aike; Part 2. Trace element and isotopic evidence bearing on the evolution of lithospheric mantle beneath southern Patagonia. In: Gurney JJ, Pascoe MD, Richardson SH (eds) *The JB Dawson volume*. Proceedings of International Kimberlite Conference 7, vol 1, pp 415–428
- Kennedy AK, Lofgren GE, Wasserburg GJ (1993) An experimental study of trace element partitioning between olivine, orthopyroxene and melt in chondrules—equilibrium values and kinetic effects. *Earth Planet Sci Lett* 115:177–195
- Kesson SE, Ringwood AE (1989) Slab-mantle interactions: 2. The formation of diamonds. *Chem Geol* 78:97–118
- Kilian R, Stern CR (2002) Constraints on the interaction between slab melts and the mantle wedge from adakitic glass in peridotite xenoliths. *Eur J Mineral* 14:25–36
- Leake BE et al (1997) Nomenclature of amphiboles: report of the subcommittee on amphiboles of the international mineralogical association, commission on new minerals and mineral names. *Can Mineral* 35:219–246
- Liu YS, Gao S, Lee CTA, Liu XM, Yuan HL (2005) Melt-peridotite interactions: links between garnet pyroxenite and high-Mg# signature of continental crust. *Earth Planet Sci Lett* 234:39–57
- Luguet A, Shirey SB, Lorand J-P, Horan MF, Carlson RW (2007) Residual platinum-group minerals from highly depleted harzburgites of the Lherz massif (France) and their role in HSE fractionation of the mantle. *Geochim Cosmochim Acta* 71:3082–3095
- Malaspina N, Hermann J, Scambelluri M, Compagnoni R (2006) Polyphase inclusions in garnet-orthopyroxenite (Dabie Shan, China) as monitors for metasomatism and fluid-related trace element transfer in subduction zone peridotite. *Earth Planet Sci Lett* 249:173–187
- McDonough WF, Sun SS (1995) The composition of the Earth. *Chem Geol* 120:223–253
- McInnes BIA, Gregoire M, Binns RA, Herzig PM, Hannington MD (2001) Hydrous metasomatism of oceanic sub-arc mantle, Lihir, Papua New Guinea: Petrology and geochemistry of fluid-metasomatised mantle wedge xenoliths. *Earth Planet Sci Lett* 188:169–183
- Nickel KG, Green DH (1985) Empirical geothermobarometry for garnet peridotites and implications for the nature of the lithosphere, kimberlites and diamonds. *Earth Planet Sci Lett* 73:158–170
- Niu YL (2004) Bulk-rock major and trace element compositions of abyssal peridotites: implications for mantle melting, melt extraction and post-melting processes beneath mid-ocean ridges. *J Petrol* 45:2423–2458
- Panman SW, Grove TL, Dann JC, del Wit MJ (2004) A subduction origin for komatiites and cratonic lithospheric mantle. *S Africa J Geol* 107:107–118
- Prouteau G, Scaillet B, Pichavant M, Maury RC (1999) Fluid-present melting of ocean crust in subduction zones. *Geology* 27:1111–1114
- Prouteau G, Scaillet B, Pichavant M, Maury R (2001) Evidence for mantle metasomatism by hydrous silicic melts derived from subducted oceanic crust. *Nature* 410:197–200
- Ramos VA, Kay SM (1992) Southern Patagonian plateau basalts and deformation: backarc testimony of ridge collision. *Tectonophysics* 205:261–282
- Rapp RP, Waston EB, Miller CF (1991) Partial melting of amphibolite/eclogite and the origin of Archean trondhjemitic and tonalites. *Precambrian Res* 51:1–25
- Ravizza G, Pyle D (1997) PGEs and Os isotopic analyses of single sample aliquots with NiS fire assay preconcentration. *Chem Geol* 141:251–268
- Roeder PL, Emslie RF (1970) Olivine-liquid equilibrium. *Contrib Mineral Petrol* 29:275–289
- Rose LA, Brenan JM (2001) Wetting properties of Fe–Ni–Co–Cu–O–S melts against olivine; implications for sulfide melt mobility. *Econ Geol* 96:145–157

- Skewes MA, Stern CR (1979) Petrology and geochemistry of alkali basalts and ultramafic inclusions from the Pali Aike volcanic field in southern Chile and the origin of the Patagonian plateau lavas. *J Volcanol Geotherm Res* 6:3–25
- Smith D, Riter JCA (1997) Genesis and evolution of low-Al orthopyroxene in spinel peridotite xenoliths, Grand Canyon field, Arizona, USA. *Contrib Mineral Petrol* 127:391–404
- Smith D, Riter JCA, Mertzman SA (1999) Water–rock interactions, orthopyroxene growth and Si-enrichment in the mantle: evidence in xenoliths from the Colorado Plateau, southwestern United States. *Earth Planet Sci Lett* 165:45–54
- Stern CR, Frey FA, Futa K, Zartman RE, Peng Z, Kyser TK (1990) Trace element and Sr, Nd, Pb, and O isotopic compositions of Pliocene and Quaternary alkali basalts of the Patagonian plateau lavas of southernmost South America. *Contrib Mineral Petrol* 104:294–308
- Stern CR, Kilian R, Olker B, Hauri EH, Kyser TK (1999) Evidence from the mantle xenoliths for relatively thin (<100 km) continental lithosphere below the Phanerozoic crust of southernmost South America. *Lithos* 48:217–235
- Toplis MJ (2005) The thermodynamics of iron and magnesium partitioning between olivine and liquid: criteria for assessing and predicting equilibrium in natural and experimental systems. *Contrib Mineral Petrol* 149:22–39
- Wang J (2007) Oxidation and metasomatism of lithospheric mantle beneath the southern South America. Unpublished PhD thesis at the University of Ottawa, p 90
- Wang J, Hattori KH, Kilian R, Stern CR (2007) Metasomatism of sub-arc mantle peridotites below southernmost South America: reduction of fO_2 by slab-melt. *Contrib Mineral Petrol* 153:607–624
- Wells PRA (1977) Pyroxene thermometry in simple and complex systems. *Contrib Mineral Petrol* 62:119–139
- Willmore CC, Boudreau AE, Kruger FJ (2000) The halogen geochemistry of the Bushveld Complex, Republic of South Africa: implications for chalcophile element distribution in the lower and critical zones. *J Petrol* 41:1517–1539
- Yoder HS, Tilley CE (1962) Origin of basalt magmas: an experimental study of natural and synthetic rock system. *J Petrol* 3:342–532
- Zhang HF, Menzies MA, Gurney JJ, Zhou XH (2001) Cratonic peridotites and silica-rich melts: diopside–enstatite relationships in polymict xenoliths, Kaapvaal, South Africa. *Geochim Cosmochim Acta* 65:3365–3377